A Circular Array for Plane-Wave Synthesis

DAVID A. HILL, FELLOW, IEEE

Abstract—**We analyze a circular array of electric line sources for generating a uniform plane wave in the interior region of the array. Identical results for the synthesized element weightings are obtained using matrix inversion or a Fourier series technique. A physical optics approximation for the element weightings is also presented, but it yields a much poorer result for the synthesized field. The angle of arrival of the plane wave can be scanned by recalculating the element weightings, and the quality of the field is maintained. Frequency scanning is also possible, but the number of array elements limits the maximum frequency.**

Key Words—**Plane-wave synthesis, uniform plane wave, antenna array.**

Index Code—**A2d, I7d.**

I. Introduction

In electromagnetic-susceptibility testing of electronic equipment, the ideal incident field is a plane wave. The feasibility of using near-field phased arrays to produce a plane wave has been studied theoretically [1], [2] and experimentally with a five-element array of horns [3] and with a seven-element array of Yagi-Uda antennas [4].

The ability to scan the direction of arrival of the plane wave electronically and to step or sweep the frequency would be extremely useful in electromagnetic-susceptibility testing. In this paper we analyze a circular array of electric line sources to study the feasibility of directional and frequency scanning. Our two-dimensional model is idealized, but it contains many of the relevant features of a more realistic three-dimensional array. Some related work with circular arrays has been performed with application to hyperthermia therapy [5]–[7] and antenna pattern measurements [8].

The organization of this paper is as follows. Section II contains a derivation of the fields produced by a circular array of line sources (the forward problem). Section III contains three methods of determining the element weightings (the inverse problem) for producing a plane wave in the interior of the circular array. Section IV contains numerical results for a number of array parameters, and Section V gives conclusions based on these numerical results.

II. Forward Problem

The geometry of the N-element circular array is shown in Fig. 1. The z-directed electric line sources are equally spaced on a circle of radius b. For this two-dimensional model, the nonzero field components are E_z, H_ρ, and H_ϕ. The electric field can be written as a superposition of the fields of the individual line sources [9]:

$$E_z = \frac{-\omega\mu}{4} \sum_{n=0}^{N-1} I_n H_0^{(2)}(k\rho_n) \tag{1}$$

where $k = \omega(\mu\epsilon)^{1/2}$, μ and ϵ are the permeability and permittivity of free space, I_n is the electric current of the nth array element, ρ_n is the distance from the nth element to the field point (ρ,ϕ), and $H_0^{(2)}$ is the zero-order Hankel function of the second kind [10]. The time dependence is exp $(j\omega t)$. We can rewrite (1) in terms of cylindrical harmonics by using the Hankel addition theorem [9]:

$$E_z = \frac{-\omega\mu}{4} \sum_{n=0}^{N-1} I_n \sum_{m=-\infty}^{\infty} H_m^{(2)}(kb) J_m(k\rho) e^{jm(\phi-\phi_n)}, \qquad \rho < b \tag{2}$$

where $\phi_n = 2\pi n/N$ and J_m is the mth-order Bessel function [10]. A similar expansion could be written for $\rho > b$.

The magnetic field components can be obtained from (2) by differentiation:

$$H_\rho = \frac{-1}{j\omega\mu\rho} \frac{\partial E_z}{\partial \phi}$$

and

$$H_\phi = \frac{1}{j\omega\mu} \frac{\partial E_z}{\partial \rho}. \tag{3}$$

If we substitute (2) into (3), we obtain

$$H_\rho = \frac{1}{4\rho} \sum_{n=0}^{N-1} I_n \sum_{m=-\infty}^{m=\infty} m H_m^{(2)}(kb) J_m(k\rho) e^{jm(\phi-\phi_n)}$$

and

$$H_\phi = \frac{jk}{4} \sum_{n=0}^{N-1} I_n \sum_{m=-\infty}^{\infty} H_m^{(2)}(kb) J_m'(k\rho) e^{jm(\phi-\phi_n)}. \tag{4}$$

For synthesis applications, we wish to optimize the field throughout a test volume of radius a, as shown in Fig. 1. We can define a hybrid vector $\boldsymbol{F}$ on the surface of this test volume [1], [2]:

$$\boldsymbol{F} = [\hat{z}E_z + \eta\hat{\rho} \times \boldsymbol{H}]|_{\rho=a} \tag{5}$$

where $\hat{z}$ and $\hat{\rho}$ are unit vectors. We have some freedom in choosing η, but we find it numerically efficient to choose it equal to the impedance of free space: $\eta = (\mu/\epsilon)^{1/2}$. For this

Manuscript received April 12, 1987.

The author is with the Electromagnetic Fields Division, National Bureau of Standards, Boulder, CO 80303. Tel. (303) 497-3472.

IEEE Log Number 8719083.

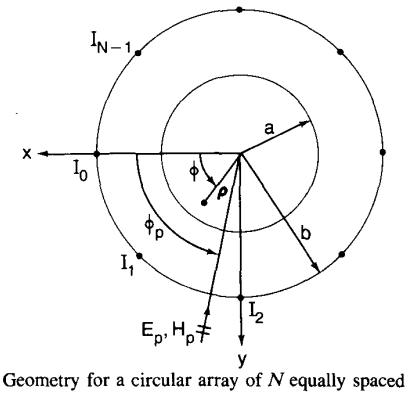

Fig. 1. Geometry for a circular array of N equally spaced elements.

two-dimensional geometry, F has only a z component:

$$F = \hat{z}F_z = \hat{z}(E_z + \eta H_\phi)|_{\rho=a}. \tag{6}$$

F_z is determined by substituting (2) and (4) into (6):

$$F_z = \frac{-k\eta}{4}\sum_{n=0}^{N-1} I_n \sum_{m=-\infty}^{\infty} H_m^{(2)}(kb) \cdot [J_m(ka) - jJ_m'(ka)]e^{jm(\phi-\phi_n)}. \tag{7}$$

III. Inverse Problem

The desired electric field is a plane wave E_{zp} propagating at an arbitrary scan angle ϕ_p to the negative x axis:

$$E_{zp} = E_0 e^{jk(x\cos\phi_p + y\sin\phi_p)} = E_0 e^{jk\rho\cos(\phi-\phi_p)} \tag{8}$$

where E_0 is a constant. If we expand the exponential in cylindrical harmonics, then (8) can be written [9]

$$E_{zp} = E_0 \sum_{m=-\infty}^{\infty} j^m e^{-jm\phi_p} J_m(k\rho)e^{jm\phi}. \tag{9}$$

The magnetic field components $H_{\rho p}$ and $H_{\phi p}$ of the plane wave can be obtained by substituting (9) into (3).

The hybrid vector for the plane wave has only a z component F_{zp} which is given by

$$F_{zp} = [E_{zp} + \eta H_{\phi p}]|_{\rho=a}. \tag{10}$$

The expansion for F_{zp} in cylindrical harmonics is

$$F_{zp} = E_0 \sum_{m=-\infty}^{\infty} j^m e^{-jm\phi_p}[J_m(ka) - jJ_m'(ka)]e^{jm\phi}. \tag{11}$$

If we equate F_z in (7) with F_{zp} in (11) and use the ϕ orthogonality of the cylindrical harmonics, then we obtain

$$\frac{-k\eta}{4} H_m^{(2)}(kb)\sum_{n=0}^{N-1} I_n e^{-jm\phi_n} = E_0 j^m e^{-jm\phi_p}, \qquad m = 0, \pm 1, \pm 2, \cdots. \tag{12}$$

To obtain (12) it was necessary to divide by the quantity $J_m(ka) - jJ_m'(ka)$. This division is always possible because this quantity has no zeros [2]. Because m ranges over all integer values from $-\infty$ to $+\infty$, we can satisfy (12) only approximately for finite N. We could actually synthesize other desired field distributions, and in such cases, the right side of (12) would be different.

A. Matrix Inversion

We can rewrite (12) in the following form:

$$\sum_{n=0}^{N-1} I_n e^{-jm\phi_n} = \frac{-4E_0 j^m e^{-jm\phi_p}}{k\eta H_m^{(2)}(kb)}. \tag{13}$$

In (13) each integer value of m provides one equation in N unknowns. We obtain the best results for the electric field if we choose the I_n values to satisfy (13) for the small $|m|$ values. Numerically, we have found no advantage to a least squares solution (number of m values greater than N). We have also found no need to constrain the I_n values [2] for this geometry. Consequently, we choose to satisfy (13) for the N smallest values of $|m|$, and this results in a system of N equations and N unknowns to be solved.

The cases of N odd or even need to be handled slightly differently, and the ranges of m values are

$$N_{\text{odd}}: m = 0, \pm 1, \pm 2, \cdots, \pm\frac{N-1}{2}$$

$$N_{\text{even}}: m = 0, \pm 1, \pm 2, \cdots, \pm\frac{N-2}{2}, +\frac{N}{2}. \tag{14}$$

Thus, we have an $N \times N$ matrix to invert, but the matrix does not depend on kb or ϕ_p. We can study the frequency-scanning (k dependence) and the angular-scanning (ϕ_p dependence) cases without having to invert a new matrix for each k or ϕ_p value.

B. Fourier Series

We can avoid matrix inversion by representing the unknown currents I_n as Fourier series. This method has been used in far-field synthesis problems with circular arrays [11]. We first write I_n in the following Fourier series form:

$$I_n = \frac{1}{N}\sum_l C_l e^{j2\pi\, ln/N}. \tag{15}$$

The unknown C_l values are called sequence currents [11], and the range of integer l values is the same as the range of the m values in (14). If we substitute (15) into (13) and reverse the order of summations, we obtain

$$\frac{1}{N}\sum_l C_l \sum_{n=0}^{N-1} e^{j2\pi(l-m)n/N} = \frac{-4E_0 j^m e^{-jm\phi_p}}{k\eta H_m^{(2)}(kb)}. \tag{16}$$

The n summation in (16) has a well-known result [11]:

$$\frac{1}{N}\sum_{n=0}^{N-1} e^{j2\pi(l-m)n/N} = \begin{cases} 1, & (l-m)/N = \text{integer} \\ 0, & \text{otherwise.} \end{cases} \tag{17}$$

Because of the restricted range of the l and m values, the summation in (17) is nonzero only for $l = m$. If we substitute (17) into (16), we obtain the following expression for the sequence currents:

$$C_m = \frac{-4E_0 j^m e^{-jm\phi_p}}{k\eta H_m^{(2)}(kb)}. \tag{18}$$

Thus, I_n is given directly by (15) and (18) without matrix inversion. We have obtained agreement between matrix inversion and the Fourier series solution to at least five digits in all our numerical results.

A remaining question is how many elements N are required to produce a reasonably uniform field inside the test volume of radius a. This question is explored numerically in Section IV, but we can also obtain an analytical estimate. The magnitude of the Bessel function $J_m(ka)$ decreases rapidly for $|m| > ka$. For N elements, we satisfy (12) for $|m|$ less than approximately $N/2$. Therefore, we require that N satisfy

$$N > 2ka. \tag{19}$$

C. Physical Optics Approximation

A physical optics approximation to the synthesis problem can be obtained by treating the array as an approximation to a continuous surface current [1]. The surface current $\boldsymbol{J}_s$ obtained from the physical optics approximation is

$$\boldsymbol{J}_s = \begin{cases} -2\hat{\boldsymbol{\rho}} \times \boldsymbol{H}_p, & -\pi/2 < \phi - \phi_p < \pi/2 \\ 0, & \text{elsewhere.} \end{cases} \tag{20}$$

If we substitute the incident plane-wave expression for $\boldsymbol{H}_p$ into (20), the surface current has only a z component J_{zs}:

$$J_{zs} = \begin{cases} -2(E_0/\eta)\cos(\phi - \phi_p) e^{jkb\cos(\phi - \phi_p)}, \\ \qquad -\pi/2 < \phi - \phi_p < \pi/2 \\ 0, \quad \text{otherwise.} \end{cases} \tag{21}$$

The element weightings I_n are obtained by sampling J_{zs}:

$$I_n = \frac{2\pi b}{N} J_{zs}|_{\phi = \phi_n}. \tag{22}$$

If we substitute (21) into (22), we obtain the physical optics approximation for I_n:

$$I_n = \begin{cases} -I_{po}\cos(\phi_n - \phi_p) e^{jkb\cos(\phi_n - \phi_p)}, \\ \qquad -\pi/2 < \phi_n - \phi_p < \pi/2 \\ 0, \quad \text{otherwise} \end{cases} \tag{23}$$

where

$$I_{po} = \frac{4\pi b E_0}{\eta N}.$$

For (23) to be valid, the array size should be large ($kb >> 1$), but the element spacings should be small ($kb/N << 1$).

IV. Numerical Results

We first consider a 16-element array ($N = 16$) of radius $b = 2\lambda$. All dimensions in this section are normalized to the free-space wavelength λ ($\lambda = 2\pi/k$). We chose N to satisfy (19) for a test volume of radius $a = \lambda$ ($2ka = 12.56$). We actually varied N over a wide range of even and odd values and found that the quality of the field produced improved slowly as N was increased. The case of $N = 16$ would be convenient for a feed network using power splitters.

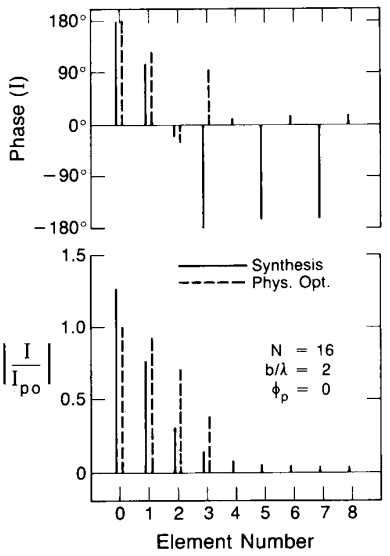

Fig. 2. Magnitude and phase of the element currents determined by synthesis and by the physical optics approximation.

In Fig. 2 we show the magnitude and phase of the synthesized currents for $\phi_p = 0$. In all cases the synthesized currents were computed by both matrix inversion and Fourier series, and the results were always identical to graphical accuracy. The simple physical optics approximation in (23) is generally quite different. In either case, the currents are normalized to I_{po}, as given by (23).The physical optics currents go to zero on the side of the array opposite from the plane-wave direction of arrival, but the synthesized currents do not. We do not show the current results for $n > 8$ because of the symmetry of the array ($I_9 = I_7$, $I_{10} = I_6$, etc.).

The magnitude of the electrical field on a radial line through the center of the test volume is shown in Fig. 3 for $\phi = 0$ and in Fig. 4 for $\phi = 90°$. The perfect plane-wave field is uniform ($|E_z/E_0| = 1$), and the synthesized field is uniform in the center of the test volume. The boundaries of the desired test volume ($\rho = \pm a$) are shown on all of the electric field plots, and the synthesized field generally deviates from a perfect plane wave near the edges. The physical optics result is generally rather poor because kb/N is not sufficiently small. The symmetry of the field in the transverse direction is apparent in Fig. 4. We do not show magnetic field plots, but they are quite similar to the electric field plots.

Corresponding phase plots are shown in Figs. 5 and 6. The phase varies nearly linearly in the longitudinal direction ($\phi = 0$) and is nearly constant in the transverse direction ($\phi = 90°$). Again, the physical optics result is poor.

We studied the angular-scanning capability of the circular array by varying the angle of arrival ϕ_p of the plane wave, and we found that the quality of the synthesized field was relatively

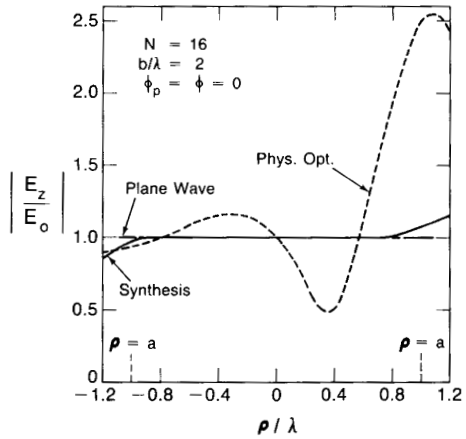

Fig. 3. Longitudinal dependence of the magnitude of the electrical field.

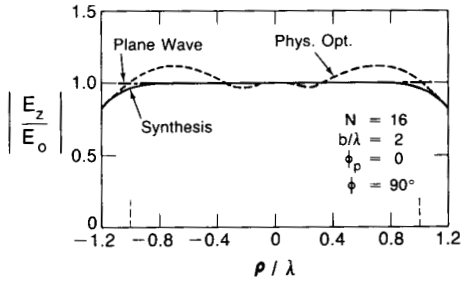

Fig. 4. Transverse dependence of the magnitude of the electrical field.

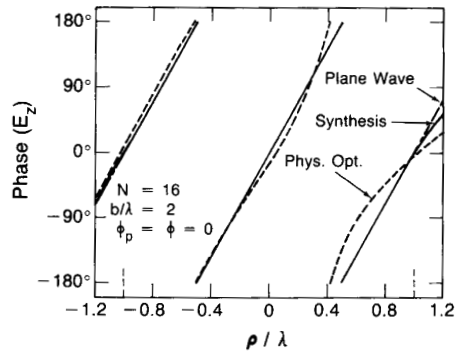

Fig. 5. Longitudinal dependence of the phase of the electrical field.

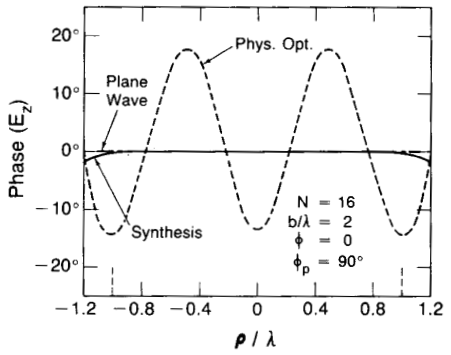

Fig. 6. Transverse dependence of the phase of the electrical field.

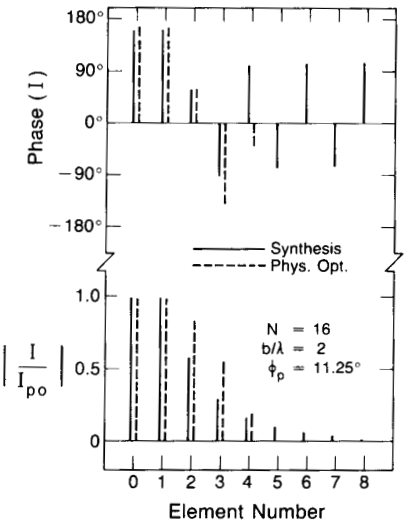

Fig. 7. Magnitude and phase of the element currents for a scan angle (ϕ_p) of 11.25°.

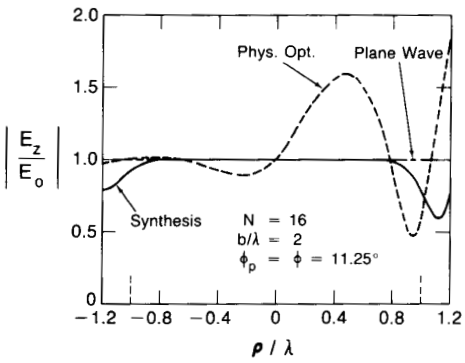

Fig. 8. Longitudinal dependence of the magnitude of the electrical field for a scan angle (ϕ_p) of 11.25°.

independent of ϕ_p. Because of the symmetry and periodicity of the array, it is sufficient to vary ϕ_p over the range, $0 \leqq \phi_p \leqq \phi_1/2$. In Fig. 7 we show the synthesized currents for $\phi_p = 11.25°$ ($= \phi_1/2$). The current values repeat for $n > 8$ ($I_9 = I_8$, $I_{10} = I_7$, etc.). Corresponding plots of the magnitude of the electric field are shown in Figs. 8 and 9. The quality of the field is comparable to that for $\phi_p = 0$ in Figs. 3 and 4. Symmetry is again apparent in the transverse direction, $\phi = \phi_p + 90° = 101.25°$. We do not show the phase results for $\phi_p = 11.25°$, but they are similar to those in Figs. 5 and 6.

We studied the frequency-scanning capability of the array by varying the frequency (wavelength) while holding N and b constant. Generally, it is necessary to recalculate the element currents I_n at each new frequency to obtain good results. If the frequency is increased enough that (19) is no longer satisfied, then the field quality is good only near the center of the test volume. To illustrate this point, we double the frequency ($b/\lambda = 4$) in Figs. 10 and 11. We now have $a/\lambda = 2$, but Fig. 11 shows that the field quality is degraded for $\rho/\lambda > 1$. In general, we find that the electrical size of the useful volume stays fairly constant as we increase the frequency so that the physical size decreases.

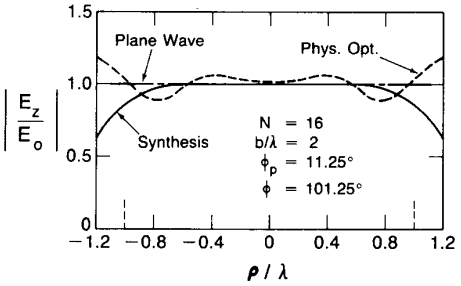

Fig. 9. Transverse dependence of the magnitude of the electrical field for a scan angle (ϕ_p) of 11.25°.

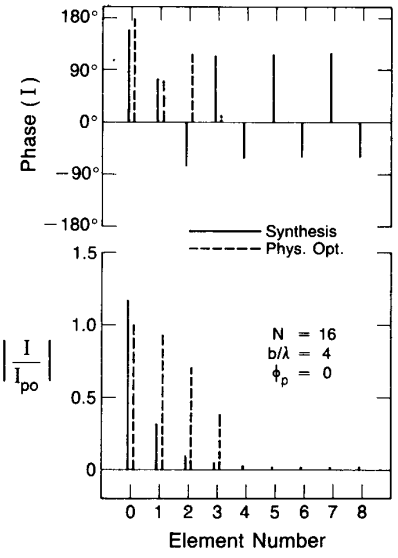

Fig. 10. Magnitude and phase of the element currents for a higher frequency.

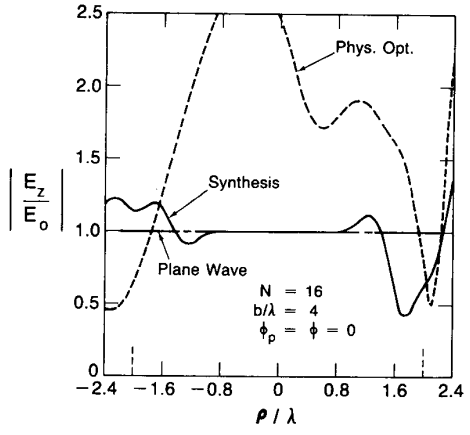

Fig. 11. Longitudinal dependence of the magnitude of the electrical field for a higher frequency.

In Figs. 12 and 13 we increase the number of elements N to 32 in order to satisfy (19). In this case the field quality is good for $\rho/\lambda < 2$. We do not show the transverse variation (ϕ = 90°) because it is typically smooth whenever the longitudinal variation (ϕ = 0) is smooth. The quality of the phase is also

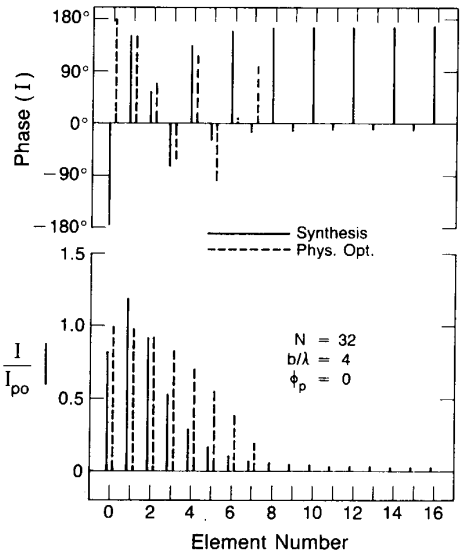

Fig. 12. Magnitude and phase of the element currents for a 32-element array.

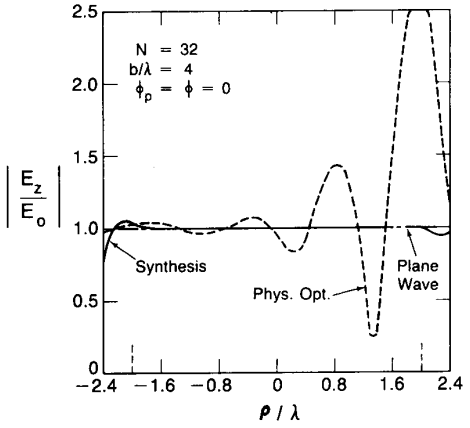

Fig. 13. Longitudinal dependence of the magnitude of the electrical field for a 32-element array.

good in these cases. The physical optics result is still poor because the requirement $kb/N << 1$ is not satisfied.

If we decrease the frequency while holding N and b constant, the results are typically quite good. To illustrate this point we halve the frequency (b/λ = 1) in Figs. 14 and 15. The field quality is good in Fig. 15, and we could probably achieve a satisfactory result with even fewer elements.

V. Conclusions

We have analyzed a circular array of electric line sources for producing a uniform plane in the interior region of the array. For this simple geometry, the synthesis technique can be greatly simplified by using a Fourier series representation for the currents, as described in Section III-B. The matrix inversion technique in Section III-A gives essentially identical results, but requires more computer time. For this geometry, no constraint on the elements was required because the fields outside the test volume did not tend to become large. The

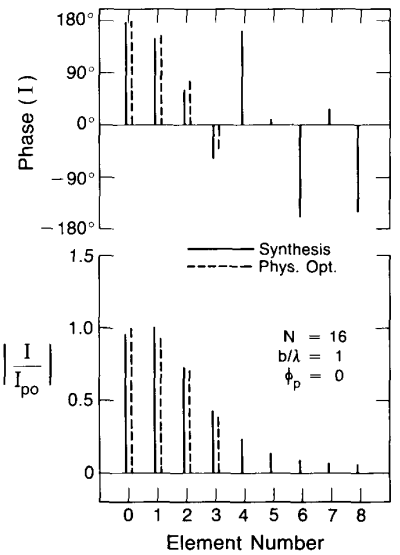

Fig. 14. Magnitude and phase of the element currents for a lower frequency.

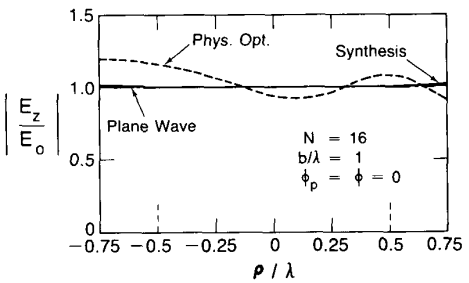

Fig. 15. Longitudinal dependence of the magnitude of the electric field for a lower frequency.

physical optics approximation provides the simplest expression for the element weightings, but it generally produces a rather nonuniform field. The synthesis results for the field were generally quite good when the number of elements satisfied (19).

Scanning the direction of arrival of the plane wave is quite feasible for this geometry, and the quality of the field is not degraded as ϕ_p is varied. Frequency scanning is also feasible as long as (19) remains satisfied. This puts a constraint on the upper frequency limit for a given number of elements. The element weightings need to be recalculated for each new frequency; so, frequency stepping would be easier than continuous scanning.

This idealized two-dimensional analysis could be extended to a more realistic three-dimensional geometry. Either a spherical [11] or a cylindrical [8] array would be interesting. In either case the near-field pattern of the array elements would need to be included in the analysis [4].

References

[1] D. A. Hill, "Theory of near-field phased arrays for electromagnetic susceptibility testing," Nat. Bur. Stand., Boulder, CO, Tech. Note 1072, 1984.

[2] D. A. Hill, "A numerical method for near-field array synthesis," *IEEE Trans. Electromagn. Compat.*, vol. EMC-27, pp. 201-211, Nov. 1985.

[3] S. K. Lynggaard, "Plane wave synthesis for antenna measurements," M.S. thesis, Tech. Univ. Denmark, Lyngby, 1982 (in Danish).

[4] D. A. Hill and G. H. Koepke, "A near-field array of Yagi-Uda Antennas for electromagnetic-susceptibility testing," *IEEE Trans. Electromagn. Compat.*, vol. EMC-28, pp. 170-178, Nov. 1986.

[5] P. F. Turner, "Regional hyperthermia with an annular phased array," *IEEE Trans. Biomed. Eng.*, vol. BME-31, pp. 106-114, 1984.

[6] J. R. Wait, "Focused heating in cylindrical targets: Part I," *IEEE Trans. Microwave Theory Tech.*, vol. MTT-33, pp. 647-649, 1985.

[7] J. R. Wait and M. Lumori, "Focused heating in cylindrical targets—Part II," *IEEE Trans. Microwave Theory Tech.*, vol. MTT-34, pp. 357-359, 1986.

[8] J. C. Bennett and N. E. Muntanga, "Antenna near-field/far-field transformation with reduced data acquisition and processing requirements," *Proc. Inst. Elec. Eng.*, vol. 129, pp. 229-231, 1982.

[9] R. F. Harrington, *Time-Harmonic Electromagnetic Fields*. New York: McGraw-Hill, 1961.

[10] M. Abramowitz and I. A. Stegun, *Handbook of Mathematical Functions*. Washington, DC: Nat. Bur. Stand., 1964.

[11] R. E. Collin and F. J. Zucker, Eds., *Antenna Theory*, part 1. New York: McGraw-Hill, 1969, sec. 5.6.

[12] A. C. Ludwig and F. H. Larsen, "Spherical near-field measurements from a compact-range viewpoint," Tech. Univ. Denmark, Lyngby, Rep. R213, 1979.